

See discussions, stats, and author profiles for this publication at: <https://www.researchgate.net/publication/231671654>

Spectral simulation of uniaxially oriented monolayers in the infrared

ARTICLE *in* **LANGMUIR** · NOVEMBER 1988

Impact Factor: 4.46 · DOI: 10.1021/la00084a024

CITATIONS

21

READS

7

2 AUTHORS, INCLUDING:



[Hatsuo Ishida](#)

Case Western Reserve University

448 PUBLICATIONS 12,896 CITATIONS

[SEE PROFILE](#)

Spectral Simulation of Uniaxially Oriented Monolayers in the Infrared

Yuichi Ishino and Hatsuo Ishida*

Department of Macromolecular Science, Case Western Reserve University,
Cleveland, Ohio 44106-1712

Received May 19, 1987. In Final Form: July 19, 1988

Ordinary and extraordinary optical constants of Langmuir-Blodgett monolayers in the infrared region were obtained by Kramers-Kronig analysis and spectroscopic ellipsometry. Based on these optical constants, internal and external reflection spectra of LB monolayers on silicon and PMMA were calculated by using the classical formulas of Drude and Fresnel. The experimental reflection spectra were identical with the spectral simulation.

Introduction

Langmuir-Blodgett (LB) monolayers^{1,2} have been studied extensively as electrical^{3,4} and optical devices^{5,6} because of the uniaxially oriented structure and the exact controllable thickness. The optically anisotropic nature of LB monolayers has been investigated in the visible⁷⁻⁹ and infrared regions.¹⁰⁻²¹ In the infrared spectra, the LB monolayer shows a remarkably anisotropic nature. The anisotropic structure of a fatty acid salt on a metallic substrate was extensively studied with reflection-absorption spectroscopy.¹²⁻¹⁷ The large difference between transmission and reflection-absorption spectra explained the anisotropic nature of LB films. The tilting angle from the surface normal was also calculated.¹² On the other hand, the anisotropic nature of infrared reflection spectra of LB monolayers on nonmetallic substrates such as semiconductors and polymers is not well explained, although some studies reported polarization ATR spectrum of LB films on germanium.^{18,19} ATR spectra obtained by using parallel and perpendicularly polarized light do not show large differences, and thus the interpretation of the spectra is sometimes difficult. The spectrum obtained by the external reflection technique of a thin film on a nonmetallic substrate shows a poor signal-to-noise (S/N) ratio and severely distorted band shapes.

A few studies have been reported^{22,23} to interpret the external reflection spectrum of thin isotropic film on nonmetallic substrates. However, there has been no study to interpret the external reflection spectrum of anisotropic films on nonmetallic substrates. The metal overlayer ATR technique was attempted in order to measure the spectrum of LB monolayers,²⁴ but there was no quantitative explanation for this technique. Therefore, even though the same material was used, because of the influence of the optical effect, the infrared spectra show different shapes when several different experimental conditions were used. This phenomena made interpreting the spectra of anisotropic thin films, such as LB monolayers, on any substrate difficult. Thus, in order to distinguish the optical effect and the chemical structural changes on the infrared spectrum of anisotropic thin film, a quantitative optical simulation of anisotropic layer will be necessary.

Recently, a method to simulate infrared spectra using several different experimental conditions was reported; this method used the Fresnel formula for isotropic films.²⁵ Also, the spectral ellipsometric technique has been utilized to determine the optical constants of thin films on metallic substrates.²⁶ In this paper, we will describe the procedure to simulate infrared reflection spectra of anisotropic

monolayers under several different experimental conditions. These calculated results will then be compared with the experimental results.

Experimental Section

IR spectra were recorded on a Digilab FTS-20E FT-IR spectrophotometer equipped with a narrow band-pass, a liquid-nitrogen-cooled mercury cadmium telluride (MCT) detector, and an ordinary broad-band IR source at a resolution of 4 cm⁻¹ throughout the region 3800–700 cm⁻¹. Coaddition of 400 scans was used. The spectrometer was purged with dry nitrogen to minimize atmospheric CO₂ and water vapor.

- (1) Blodgett, K. B. *J. Am. Chem. Soc.* 1935, 57, 1007.
- (2) Blodgett, K. B.; Langmuir, I. *Phys. Rev.* 1937, 51, 964.
- (3) Dowa, A. S.; Fung, C. D.; Dipoto, E. P.; Rickert, S. E. *Thin Solid Films* 1985, 132, 27.
- (4) Fung, C. D.; Larkins, G. L. *Thin Solid Films* 1985, 132, 33.
- (5) Pitt, C. W.; Walpita, R. M. *Thin Solid Films* 1980, 68, 101.
- (6) Barnes, W. L.; Sambles, J. R. *Surf. Sci.* 1986, 177, 399.
- (7) den Engelsen, D. *J. Opt. Soc. Am.* 1971, 61, 1460.
- (8) Swalen, J. D.; Rieckhoff, K. E.; Tacke, M. *Opt. Commun.* 1978, 24, 146.
- (9) Pockland, I.; Swalen, J. D.; Gordon, J. G., II; Philpott, M. R. *Surf. Sci.* 1977, 74, 237.
- (10) Chollet, P.; Messier, J.; Rosillio, C. *J. Chem. Phys.* 1976, 64, 1042.
- (11) Chollet, P. *Thin Solid Films* 1978, 52, 343.
- (12) Allara, D. L.; Swalen, J. D. *J. Phys. Chem.* 1982, 86, 2700.
- (13) Knoll, W.; Philpott, M. R.; Golden, W. G. *J. Chem. Phys.* 1982, 77, 219.
- (14) Golden, W. G.; Snyder, D.; Smith, B. *J. Phys. Chem.* 1982, 86, 4675.
- (15) Golden, W. G.; Saperstein, D. D. *J. Electron Spectrosc. Relat. Phenom.* 1983, 30, 43.
- (16) Rabolt, J. F.; Barns, F. C.; Schlotter, N. E.; Swalen, J. D. *J. Chem. Phys.* 1983, 78, 946.
- (17) Rabolt, J. F.; Barns, F. C.; Schlotter, N. E.; Swalen, J. D. *J. Electron Spectrosc. Relat. Phenom.* 1983, 30, 29.
- (18) Takenaka, T.; Nogami, K.; Gotoh, H.; Gotoh, R. *J. Colloid Interface Sci.* 1971, 35, 395.
- (19) Takenaka, T.; Nogami, K.; Gotoh, H. *J. Colloid Interface Sci.* 1972, 40, 409.
- (20) Ohnishi, T.; Ishitani, T.; Ishida, H.; Yamamoto, N.; Tsubomura, T. *J. Phys. Chem.* 1978, 82, 1989.
- (21) Ohta, K.; Iwamoto, R. *Anal. Chem.* 1985, 57, 2491.
- (22) Porter, M. D.; Bright, B.; Allara, D. L.; Kuwana, T. *Anal. Chem.* 1986, 58, 2461.
- (23) Udagawa, A.; Matsui, T.; Tanaka, S. *Appl. Spectrosc.* 1986, 40, 793.
- (24) Sigarev, A. A.; Yakovlev, V. A. *Opt. Spectrosc.* 1984, 56, 336.
- (25) Graf, R. T.; Koenig, J. L.; Ishida, H. In *FT-IR Characterization of Polymers*; Ishida, H., Ed.; Plenum: New York, 1987; p 385.
- (26) Graf, R. T.; Koenig, J. L.; Ishida, H. *Anal. Chem.* 1986, 58, 64.

* Author to whom correspondence should be addressed.

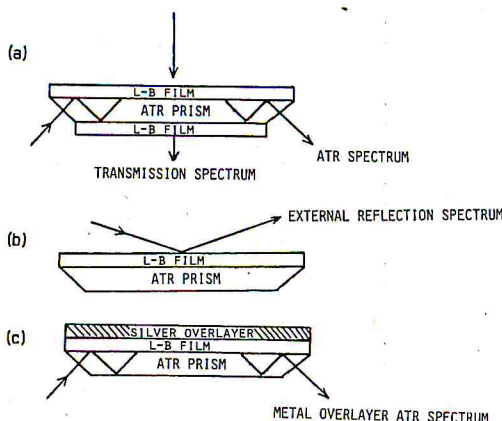


Figure 1. Sample setup for (a) transmission and ATR, (b) external reflection, and (c) metal overlayer techniques.

A cadmium arachidate (CdA) monolayer film was deposited on a silicon ATR trapezoidal element ($50 \times 10 \times 2$ mm) which was treated with hexamethyldisilazane (HMDS) by using the Langmuir-Blodgett (LB) deposition technique in a class 10 clean room.²⁷ This LB film was used for transmission, ATR, external reflection, and the metal overlayer ATR technique (Figure 1). For the transmission and ATR experiments, we used an LB film on both sides of the ATR element. For the external reflection technique, we removed the film from one side of the ATR element using a cotton swab immersed in chloroform. For the metal overlayer ATR technique, silver is evaporated on the LB film on a silicon ATR element in a vacuum. For this experiment, there was no film on the other side of ATR element. The thickness of the silver layer was calculated from the amount of silver in the tungsten basket and the distance between the tungsten basket and the ATR element. The LB film for the ellipsometry technique was deposited on the vacuum-evaporated silver film on a glass microscope slide. For this experiment, HMDS treatment was done before the deposition of the LB film. An LB film on a poly(methyl methacrylate) (PMMA) plate was prepared by using the same technique, except the HMDS treatment was not used for PMMA substrate.

For the ATR and metal overlayer ATR measurements, Wilks' ATR attachment was used. An external reflection measurement was made with Harrick's external reflection attachment at several incident angles. Static ellipsometry measurements were performed based on the method reported by Graf et al.,²⁸ using two polarizers before and after the external reflection attachment.

A uniaxially oriented medium has two refractive indices: the ordinary refractive index and the extraordinary refractive index.²⁸ The ordinary refractive index (n_o) is the refractive index for the electric vector perpendicular to the optical axis of the anisotropic medium. The extraordinary refractive index (n_e) is for the electric vector parallel to the optical axis. Also, there are ordinary and extraordinary extinction coefficients (k_o and k_e). Therefore, the ordinary and extraordinary complex refractive indices can be expressed as $n_o = n_o - ik_o$ and $n_e = n_e - ik_e$.

For the calculation of optical constants of an LB film in the infrared, ordinary and extraordinary refractive indexes at 612 nm and the thickness of the monolayer obtained by Pitt et al.²⁹ were used. Optical constants of PMMA were obtained by Kramers-Kronig analysis³⁰ on the transmission spectrum of a free-standing film. The calculation of the electric field intensity is based on Hansen's algorithm.³¹

The computer program for the calculation of optical constants by the Kramers-Kronig analysis, ellipsometric equations, electric field intensity, and reflectivity of stratified layers including a uniaxially oriented layer was written in FORTRAN 77 on a Digital

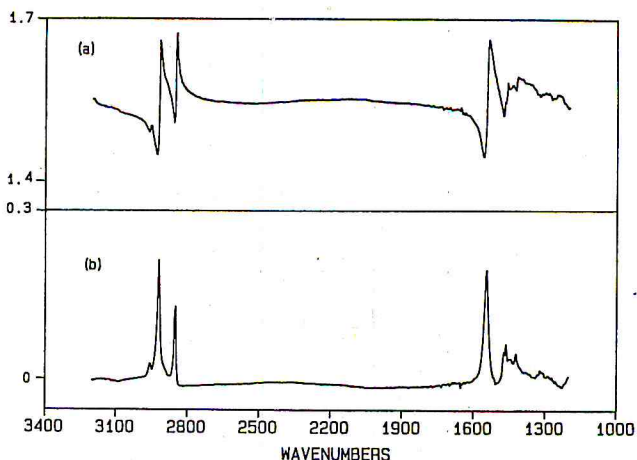


Figure 2. Ordinary (a) refractive index and (b) extinction coefficient of CdA LB film.

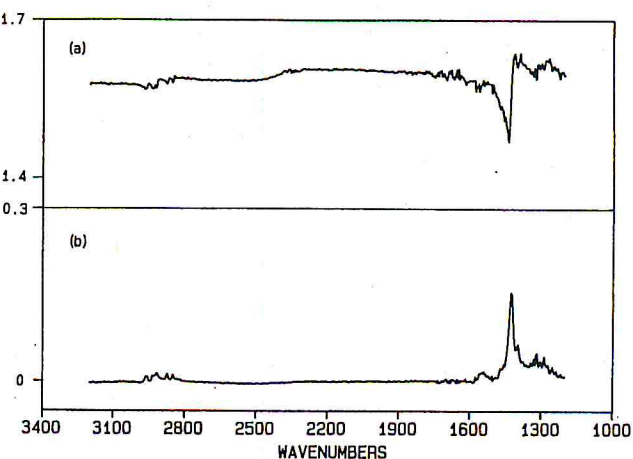


Figure 3. Extraordinary (a) refractive index and (b) extinction coefficient of CdA LB film.

Equipment Corp. VAX/VMS 11-780 system.

Results and Discussion

When Langmuir-Blodgett monolayers are deposited on an isotropic substrate, the plane of incidence is parallel to the optical axis of the LB film. It is well-known that in the case of transmission spectroscopy of a thin film on a transparent substrate the transition dipole moment of the thin film interacts with the electric vector which is parallel to the surface of thin film. On the other hand, in the case of reflection-absorption spectroscopy of thin films on metallic substrates, only the electric vector which is parallel to the plane of incidence interacts with the transition dipole moment of the thin film normal to the substrate surface. Because of this, we can measure the ordinary complex refractive index with transmission spectroscopy and the extraordinary complex refractive index with reflection-absorption spectroscopy.

In order to obtain the ordinary refractive index and extinction coefficient (Figure 2), the transmission spectrum of 40 layers of cadmium arachidate (CdA) LB monolayers on a silicon substrate was measured. From the transmission spectrum and thickness of the monolayer, the extinction coefficient was first obtained, and then the refractive index was calculated by the Kramers-Kronig analysis.

In order to measure the extraordinary refractive index and extinction coefficient (Figure 3), a static ellipsometric measurement of a CdA LB film on a silver substrate was performed. The first polarizer before the reflection at-

(27) Biddle, M. B.; Rickert, S. E.; Lando, J. B. *Thin Solid Films* 1985, 134, 121.

(28) See, e.g., Azaam, R. M.; Bashara, N. M. *Ellipsometry and Polarized Light*; North-Holland: Amsterdam, 1977.

(29) Pitt, C. W.; Walpita, L. M. *Electron. Lett.* 1976, 12, 479.

(30) Graf, R. T.; Koenig, J. L.; Ishida, H. *Appl. Spectrosc.* 1985, 39, 405.

(31) Hansen, W. N. *J. Opt. Soc. Am.* 1968, 58, 380.

tachment is set with its azimuthal angle at 45° . The second polarizer after the reflection attachment, i.e., the analyzer, was set with its azimuthal angle at 0° , 90° , 45° , and -45° , at which R_p , R_s , R_{45} , and R_{-45} were measured, respectively. When the above four reflectivities were measured on the evaporated silver film on a glass microscope slide, optical constants of substrate were calculated by the following equations:³²

$$\frac{R_p}{R_s} = \tan^2 \psi \quad (1)$$

$$\frac{R_{-45}}{R_{45}} = \frac{1 - \sin^2 \psi \cos \Delta}{1 + \sin^2 \psi \cos \Delta} \quad (2)$$

$$n^2 - k^2 = \sin^2 \theta \left[1 + \frac{(\tan^2 \theta)(\cos^2 2\psi - \sin^2 2\psi \sin^2 \Delta)}{(1 + \sin 2\psi \cos \Delta)^2} \right] \quad (3)$$

$$2nk = \frac{\sin^2 \theta \tan^2 \theta \sin^4 \psi \sin \Delta}{(1 + \sin^2 \psi \cos \Delta)^2} \quad (4)$$

By using these optical constants of the substrate and the four reflectivities of 20 layers of CdA LB film on silver, we calculated the extraordinary complex refractive index of CdA LB monolayers with the nonlinear least-squares refinement procedure.³³

When ordinary (Figure 2) and extraordinary extinction coefficients (Figure 3) are compared, the peak intensity of the carboxylate antisymmetric stretching mode in the ordinary extinction coefficient (k_o) is larger than that of the carboxylate symmetric stretching mode in the extraordinary extinction coefficient (k_e). Hence, if the same electric field intensity is applied for the parallel and perpendicular directions, it is expected that the antisymmetric stretching mode will have a larger intensity than that of the symmetric stretching mode. However, in order to simulate valid reflection spectra of an LB film under several experimental conditions, eq 5–10 need to be applied. For the spectral simulation of reflection measurements of stratified layers containing an anisotropic layer, Fresnel's reflection coefficients for boundaries between an isotropic layer and an anisotropic layer are expressed by Drude's formula:³⁴

$$r_{(i-1)pp} = \frac{n_{io} n_{ie} \cos \theta_{i-1} - n_{i-1} (n_{ie}^2 - n_{i-1}^2 \sin^2 \theta_{i-1})^{1/2}}{n_{io} n_{ie} \cos \theta_{i-1} + n_{i-1} (n_{ie}^2 - n_{i-1}^2 \sin^2 \theta_{i-1})^{1/2}} \quad (5)$$

$$r_{i(i+1)pp} = \frac{-n_{io} n_{ie} \cos \theta_{i+1} - n_{i+1} (n_{ie}^2 - n_{i+1}^2 \sin^2 \theta_{i+1})^{1/2}}{n_{io} n_{ie} \cos \theta_{i+1} + n_{i+1} (n_{ie}^2 - n_{i+1}^2 \sin^2 \theta_{i+1})^{1/2}} \quad (6)$$

$$r_{(i-1)ss} = \frac{n_{i-1} \cos \theta_{i-1} - (n_{io}^2 - n_{i-1}^2 \sin^2 \theta_{i-1})^{1/2}}{n_{i-1} \cos \theta_{i-1} + (n_{io}^2 - n_{i-1}^2 \sin^2 \theta_{i-1})^{1/2}} \quad (7)$$

$$r_{i(i+1)ss} = \frac{-n_{i+1} \cos \theta_{i+1} - (n_{io}^2 - n_{i+1}^2 \sin^2 \theta_{i+1})^{1/2}}{n_{i+1} \cos \theta_{i+1} + (n_{io}^2 - n_{i+1}^2 \sin^2 \theta_{i+1})^{1/2}} \quad (8)$$

Similarly, phase thickness becomes

$$\beta_{ip} = 2\pi(d_i/\lambda)(n_{io}/n_{ie})(n_{ie}^2 - n_{i-1}^2 \sin^2 \theta_{i-1})^{1/2} \quad (9)$$

$$\beta_{is} = 2\pi(d_i/\lambda)(n_{io}^2 - n_{i-1}^2 \sin^2 \theta_{i-1})^{1/2} \quad (10)$$

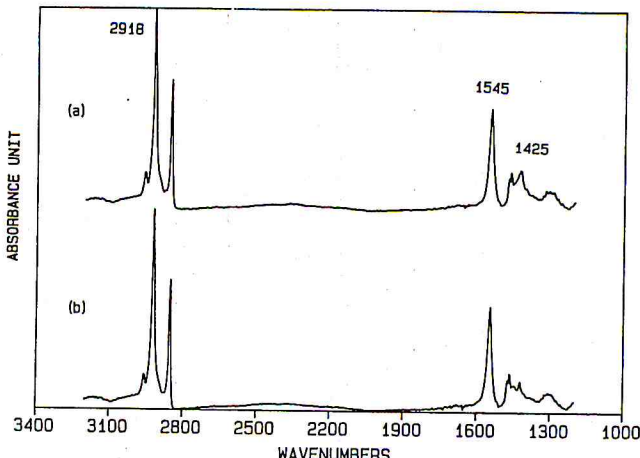


Figure 4. Simulated ATR spectrum of CdA 20-layer LB film on a silicon ATR prism at 45° , obtained by using (a) parallel polarized and (b) perpendicularly polarized light.

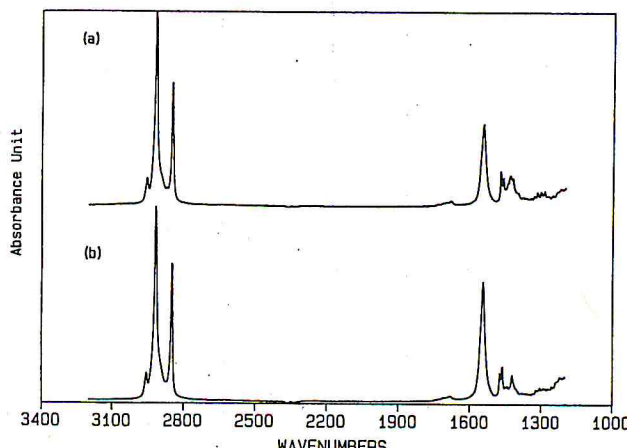


Figure 5. Experimental ATR spectrum under the same conditions as in Figure 4.

where $r_{(i-1)pp}$ is the reflection coefficient for the boundary between the i th and the $(i-1)$ th phase for parallel polarization, $r_{(i-1)ss}$ the reflection coefficient for the boundary between the i th and the $(i-1)$ th phase for perpendicular polarization, n_i the complex optical constant for the i th phase, β_{ip} the phase thickness of the i th phase for parallel polarization, β_{is} the phase thickness of the i th phase for perpendicular polarization, d_i the thickness of the i th phase, θ_i the angle of incidence or refraction for the i th phase, and λ the wavelength.

In order to obtain reflectivity values for the ATR measurement, Fresnel's formula for a three-layered stratified system may be used. For an anisotropic layer, the reflectivity coefficients mentioned above need to be used. The refractive index of silicon is assumed to be 3.42 in the infrared range, and the extinction coefficient is determined by the transmission spectrum of a silicon plate. Figure 4 shows the simulated ATR spectrum of the 20 layers of CdA LB film on a silicon ATR prism. As shown in this spectrum, when 45° is used as the angle of incidence the ATR spectrum with parallel polarized light shows a small band of symmetric carboxylate stretching (1425 cm^{-1}), but the ATR spectrum with perpendicularly polarized light does not show that band. However, the difference between the two spectra is small, although the dipole moments of these vibration modes are perpendicular to each other.

This fact can be explained by the field intensity of an evanescent wave. Figure 6 shows the angular dependence of the electric field at the surface of a prism, where the z -axis is surface normal and the y -axis is perpendicular to

(32) Roseler, A.; Molgedey, W. *Infrared Phys.* 1984, 24, 1.

(33) Cameron, D. G.; Escobar, D.; Goplen, T. G.; Jones, R. N. "Computer Programs for Infrared Spectrophotometry, Bulletin No. 17"; National Research Council, Canada, 1977; p 67.

(34) Abeles, F.; Washburn, H. A.; Soonpaa, H. H. *J. Opt. Soc. Am.* 1973, 63, 104.

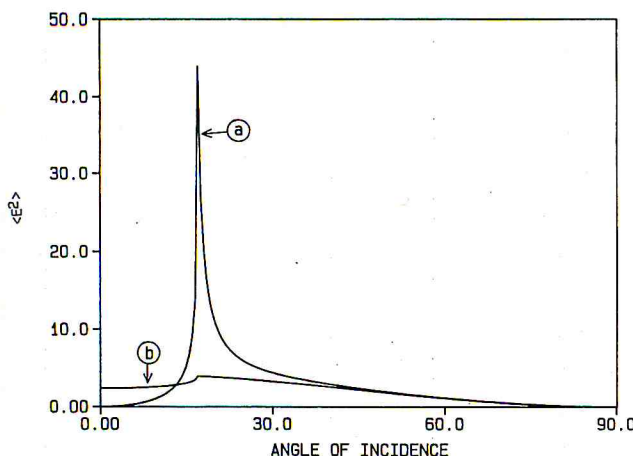


Figure 6. Angular dependence of electric field intensity at the surface of silicon prism. In the case of internal reflection of the silicon-air system, a and b show $\langle E_z^2 \rangle$ and $\langle E_y^2 \rangle$, respectively.

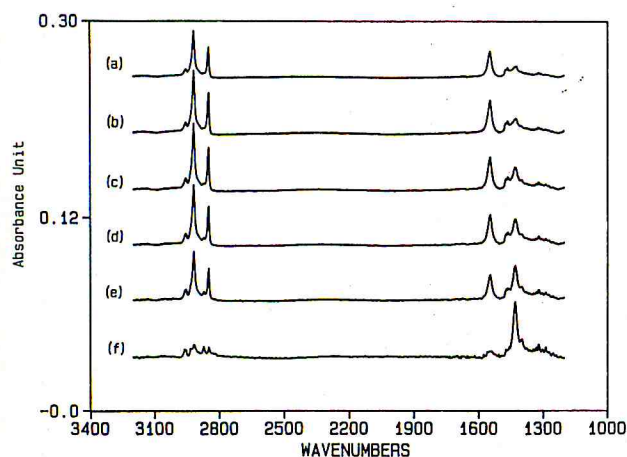


Figure 7. Simulated ATR spectrum of CdA LB film, obtained by using parallel polarized light at several angles of incidence: (a) 45°, (b) 30°, (c) 20°, (d) 19°, (e) 18°, and (f) 17°.

the plane of incidence and the propagation vector. As shown in this figure, the field intensity of the parallel component (E_z) is similar to that of the perpendicular component (E_y) at 45°. Figure 5 shows the experimental ATR spectrum under the same conditions. The simulation utilizing Drude's formula is quite successful since the experimental spectrum is almost identical with the calculated spectrum.

The angular dependence of the ATR spectra can be calculated by using the same procedure. In order to measure the angular dependence of the ATR spectrum by actual experiment, many kinds of trapezoidal ATR elements with different acute angles are needed, except for the case where multiple reflections are sacrificed by using a hemicylinder element with a single reflection. Thus, the simulation of angular dependence of the ATR spectrum is worthwhile. Figure 7 shows the change of ATR spectrum obtained by using parallel polarized light at several angles of incidence. The interesting point appears when the angle of incidence becomes close to the critical angle. The intensity of the carboxylate symmetric stretching mode increases, but that of the antisymmetric stretching mode decreases. Also, the intensity of the CH_2 stretching modes (2918 and 2850 cm^{-1}) decreases. This fact can be explained by the strong field intensity of the z-component at the critical angle (Figure 6). Therefore, to verify the orientation of molecules, the angle of incidence has to be close to the critical angle, since this condition is more sensitive for the orientation than the higher angle of incidence.

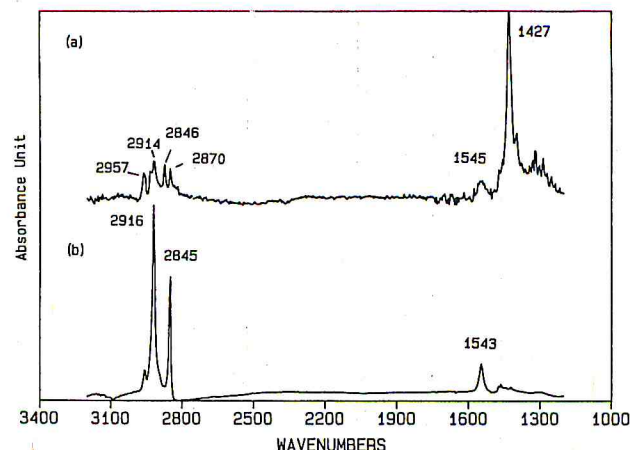


Figure 8. Simulated ATR spectrum of 10 monolayers of CdA LB film between a silicon prism and a silver 20-nm overlayer at 45°, obtained by using (a) parallel and (b) perpendicularly polarized light.

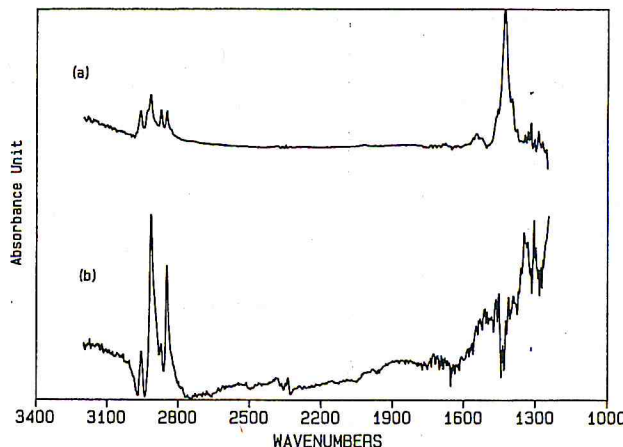


Figure 9. Experimental metal overlayer ATR spectrum obtained under the same conditions as Figure 8.

Metal overlayer ATR spectroscopy has been demonstrated to enhance the intensity of the spectrum of a very thin film. However, if a silver overlayer is placed on the CdA LB film on the silicon ATR element, the ATR spectrum observed at 45° is totally changed. This is also predicted by the spectral simulation. In this case we are dealing with a four-layered system (silicon-LB film-silver-air), and Fresnel's equation for a four-layered system is applicable. For this calculation, the optical constant of silver is calculated from Drude's free electron theory.³⁵ Figure 8 is the simulated ATR spectrum of 10 monolayers of a CdA LB film between a silicon prism and a silver 20-nm overlayer. As shown in Figure 8, when parallel polarized light is used the carboxylate symmetric stretching band (1427 cm^{-1}) is the most intensive. When perpendicularly polarized light is used, the CH_2 stretching mode (2916 and 2845 cm^{-1}) is the most intense band. In other words, the effect of the extraordinary extinction coefficient is dominant in the spectrum of parallel polarized light, whereas the effect of the ordinary extinction coefficient is dominant in the spectrum of perpendicularly polarized light. Experimental results (Figure 9) also show the same trend, except that a poor S/N ratio in the spectrum of perpendicularly polarized light is seen. For metal overlayer ATR spectroscopy, since the z-component of the electric field intensity is dominant at the gap between prism and

(35) Johnson, P. B.; Christy, R. W. *Phys. Rev. B: Condens. Matter* 1972, 6, 4370.

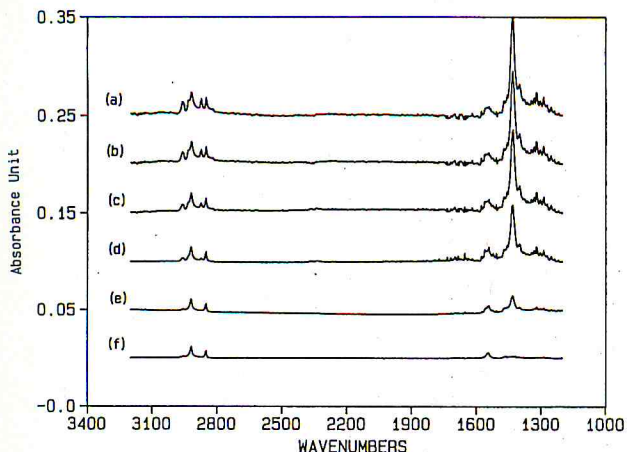


Figure 10. Simulation of metal overlayer ATR spectrum at 45°, with a silver overlayer thickness of (a) 5, (b) 4, (c) 3, (d) 2, and (e) 1 nm and (f) without a silver layer. Parallel polarized light is used.

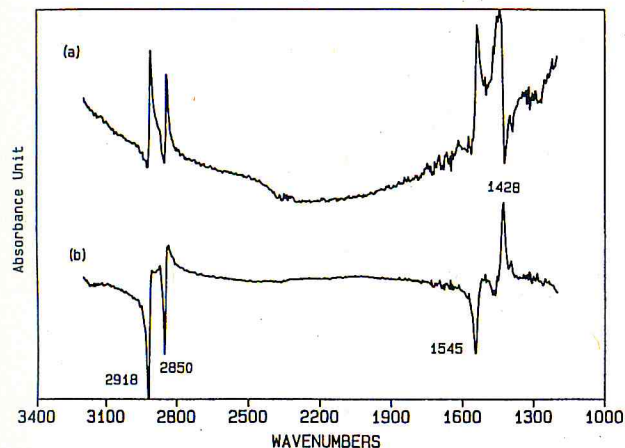


Figure 11. Simulated external reflection spectra of CdA 20-layer LB film on a silicon substrate at (a) 75° and (b) 60°. Parallel polarized light is used.

silver, parallel polarized light gives better sensitivity.

For this metal overlayer experiment, controlling the thickness of the silver layer is experimentally difficult, and the further prediction of the spectral changes occurring for the different thickness of the silver overlayer is worthwhile. Figure 10 shows the simulation for the metal overlayer ATR spectrum for various thicknesses of the silver overlayer. As the thickness of the silver overlayer increases, the absorbance of the carboxylate symmetric stretching and methyl CH₃ stretching modes (2957 and 2846 cm⁻¹) increases. When the silver overlayer is 5 nm, the absorbance of the carboxylate symmetric stretching is maximum. Therefore, the optimum thickness of the silver layer to obtain the best S/N ratio can be predicted by the spectral simulation. In this case, however, the determination of the optical constants of silver is difficult. When the silver is evaporated in a vacuum, the silver film consists of silver islands. Therefore, the optical constants of the silver layer have to be carefully examined.

External reflection spectroscopy of an LB film on a nonmetallic substrate shows the most complex spectrum. Figure 11 shows the simulated external reflection spectra of 20 layers of CdA LB film on a silicon substrate at 60° and 75°, obtained with the parallel polarized light. The simulated spectrum at 60° shows a negative CH₂ stretching mode (2918 and 2850 cm⁻¹), a negative carboxylate antisymmetric stretching mode (1545 cm⁻¹), and a positive carboxylate symmetric stretching mode (1428 cm⁻¹). On

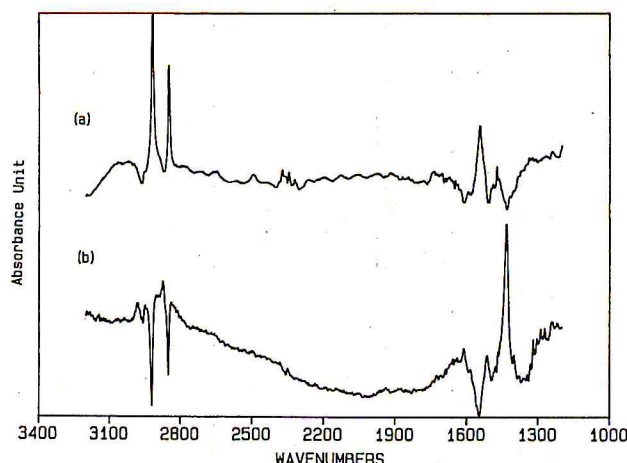


Figure 12. Experimental external reflection spectrum obtained under the same conditions as Figure 11.

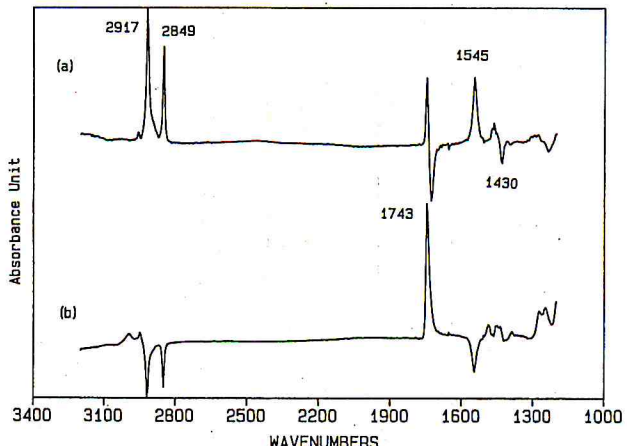


Figure 13. Simulated external reflection spectra of CdA 40-layer LB film on PMMA substrate at 75°, obtained by using (a) parallel and (b) perpendicularly polarized light.

the other hand, at 75° a positive CH₂ stretching mode and a carboxylate antisymmetric stretching mode are seen, and carboxylate symmetric stretching is very distorted. Actually, the experimental spectra under the same conditions show similar spectra (Figure 12). Small differences between calculation and experiment may be expected because of angular dispersion of the incident beam and a poor S/N ratio. However, this complex spectrum is obviously due to the optical effect on the spectrum of anisotropic thin film. The appearance of the positive and negative peaks of an LB film at the same angle is due to anisotropic optical constants. This effect can be explained by the shift of angle of minimum reflectivity, which is called Brewster's angle when there is no film on the silicon. The existence of the extraordinary complex refractive index makes the angle of minimum reflectivity lower, and an ordinary complex refractive index makes the angle of minimum reflectivity higher than the Brewster angle of the silicon substrate. Since in this system the existence of the LB film does not make the large change on the reflectivity, the reflectivity curve of the parallel polarized light of the LB film on silicon intersects with that of the bare silicon near the Brewster angle. Therefore, some bands show positive and negative absorbances around the Brewster angle of the silicon (73.7°). Also, the LB film on the silicon wafer shows similar characteristics in the external reflection spectrum.³⁶

(36) Tan, J. M. M.S. Thesis, Case Western Reserve University, Cleveland, OH, 1986.

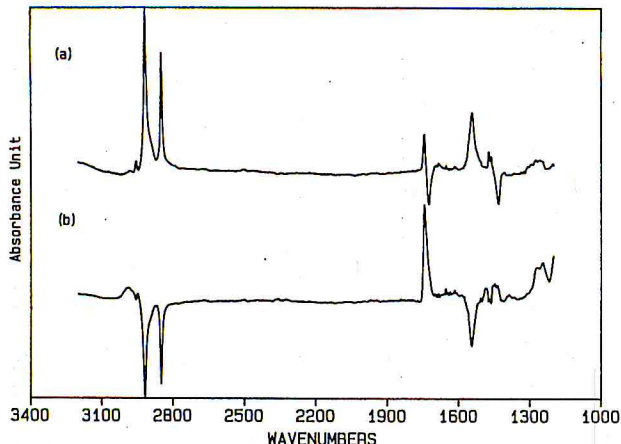


Figure 14. Experimental external reflection spectrum obtained under the same conditions as Figure 13.

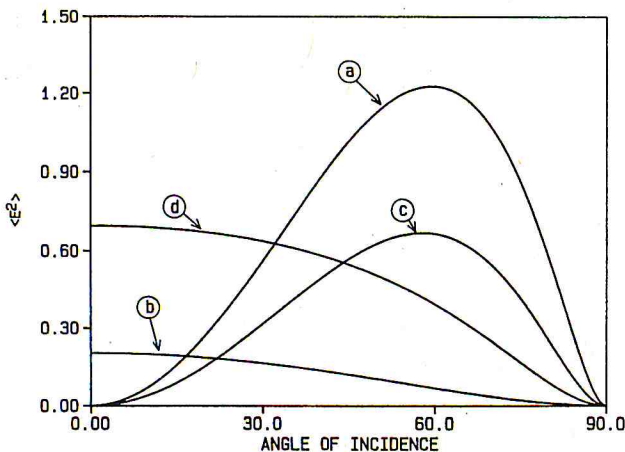


Figure 15. Angular dependence of electric field intensity at the surface of the substrate for the case of external reflection: (a) $\langle E_z^2 \rangle$ of air-silicon, (b) $\langle E_y^2 \rangle$ of air-silicon, (c) $\langle E_z^2 \rangle$ of air-PMMA, and (d) $\langle E_y^2 \rangle$ of air-PMMA.

When PMMA is used as the substrate, the external reflection spectrum of an LB film shows other features. Figure 13 shows the simulated external reflection spectra of 40 layers of a CdA LB film on a PMMA substrate, obtained by using parallel and perpendicularly polarized lights. In this case, even when parallel polarized light is

used, only the weak negative carboxylate symmetric stretching mode (1430 cm^{-1}) is observed at 75° . This fact is due to the lower intensity of the z -component of the electric field on the PMMA substrate compared to that on the silicon substrate (Figure 15). When perpendicularly polarized light is used, the spectrum due to the LB film shows negative absorbances. In these simulated spectra, the denominator of the absorbance unit is the reflectivity of the bare PMMA plate, so that the absorbance of the substrate is theoretically compensated. However, as shown in Figure 13, residual absorbance of the substrate remains as a positive absorbance on the spectrum of the perpendicularly polarized light. The experimental spectrum (Figure 14) shows an spectrum identical with the simulation spectrum. Therefore, it can be concluded that the structure of LB film on PMMA substrate is identical with the structure of LB film on silicon and silver substrates. In the case of PMMA substrate, at a lower angle than Brewster's angle there is no carboxylate symmetric stretching mode observed because the z -component of the electric field is less intensive than the y -component (Figure 15). Thus, in order to determine the anisotropy of an LB film on PMMA a higher angle of incidence than Brewster's angle is preferred. For the external reflection spectrum on a nonmetallic substrate, the intensity ratio of the carboxylate symmetric and antisymmetric stretching modes, which shows negative and positive direction of peak respectively, can be used as the index of the anisotropy.

Conclusion

The use of spectral simulation according to the formula of Drude and Fresnel is quite successful in predicting the actual infrared spectra of LB monolayers on different substrates and under different experimental conditions. By comparing the simulated spectrum to the actual spectrum, the optical effect and the chemical effect on the spectral change can be distinguished. Thus, the structure of uniaxially oriented molecule on any substrate can be determined by using this spectral simulation.

Acknowledgment. We gratefully acknowledge the partial financial support of the Bridgestone Corp. We also thank J. M. Tan, Case Western Reserve University, for providing LB films used.

Registry No. CdA, 14923-81-0; PMMA, 9011-14-7; Si, 7440-21-3.